

# Static Cyclic Loading Test on Moment Resisting Frame with Slab Simulating Seismic Performance of High-Rise Reinforced Concrete Buildings



**Toshikazu Kabeyasawa**

*National Institute for Land, and Infrastructure Management, Japan*

**H. Fukuyama**

*Building Research Institute, Japan*

**D. Xuan & Toshimi Kabeyasawa**

*Earthquake Research Institute, University of Tokyo, Japan*

**H. Katsumata & K. Sugimoto**

*Technical Research Institute, Obayashi Corporation, Japan*

## SUMMARY:

This paper presents experimental and analytical responses of two-fifth scale three-dimensional reinforced concrete frame with floor slab under seismic loading. The test specimen was constructed with four columns and two frames in both directions to simulate the seismic performance of moment-resisting frames with slab in the high-rise buildings. A special loading set-up was developed to simulate the boundary conditions in medium-story frame so that the axial elongation of the beams would not be constrained by the reaction supports. The damage patterns as well as the lateral resistances of the frames in various inter-story drift ratios were investigated considering the contributions of the slab to the beam resistance. It was found from the test that the strain of slab reinforcing bars were increasing almost uniformly through the whole slab width and was fully effective to the flexural strength of the beams at one percent story drift and after.

*Keywords: high-rised reinforced concrete buildings, effective slab width, sub-assembly, beam elongation*

## 1. INTRODUCTION

Current design practice of high-rise building in Japan is based on the capacity design concept, where the formation of desirable beam-yielding overall collapse mechanism is to be ensured considering the realistic inelastic behavior of structural components. Because the beam flexural strengths are affected by the slab, the effective slab width is regulated in the standards and guidelines with conservative values so as not to overestimate the ultimate lateral loading capacity at the beam-yielding mechanism. However, the conservative slab width would not always be safe assumption in ensuring the mechanism. Therefore, the accurate evaluation on the effective slab width, especially in relation with inter-story drift is still essential in modeling the frame structures.

On the other hand, the experimental verifications were conducted in the 1980s and the early of 1990s, such as with beam-column subassembly tests (Suzuki, Otani and Kobayashi (1984)) and frame subassembly tests (Sakata et al. (1989)), by which the whole slab width could be effective although the drift level was relatively large. Also these previous tests indicated that the slab participation might have been influenced by the boundary and loading conditions in the tests.

Therefore, the test was planned using the three-dimensional specimen with four columns and two frameworks in both directions, simulating the realistic boundary condition of slab in high-rise buildings. Special consideration on the boundary conditions at the column bases was also taken into account so that the axial elongations in the beams would not be constrained by the columns but only with tensile reaction of the slab. The test results have been reported elsewhere, while the contribution of slab to the beam resistance is discussed here in details.

## 2. TEST SPECIMEN

### 2.1. Specimen

This specimen represents the interior part of high-rise buildings' middle stories as shown in Fig. 1. Four columns of the sub-assembly were extended to certain height to situate test conditions of laboratory. The beams in each direction include one span and two half-spans with floor slabs. Two end beams were added for the installation of pin supports at the ends.

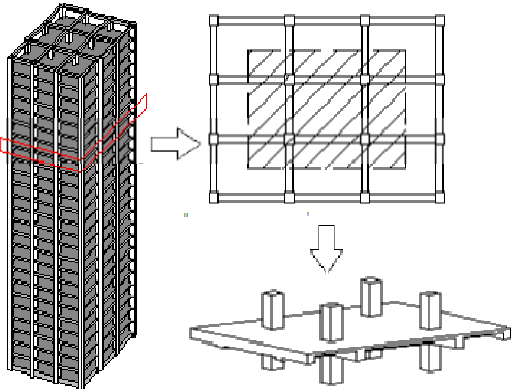


Figure 1. Modeling concept of the specimen

The height of the specimen is 2010mm with 1085mm upper columns and 925mm lower columns measured from the beam's center axis as shown in Fig. 2. In the longitudinal direction, the center-to-center middle span is 3200mm; center-to-end half-span is 1710mm. In transverse direction, the center-to-center middle span is 2500mm; center-to-end half-span is 1100mm. The column sectional dimensions were 400mm by 400mm. The sections of the longitudinal and transverse beams were 300mm by 360mm. The sections of the transverse beam at the ends were 220mm by 290mm. The slab thickness was 100mm.

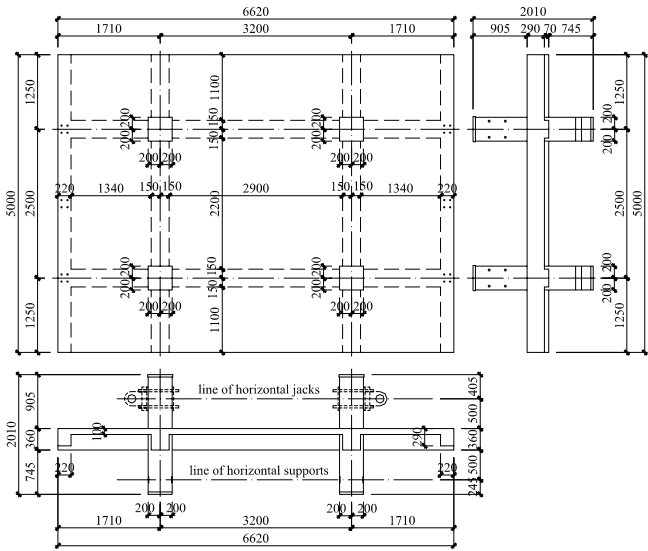
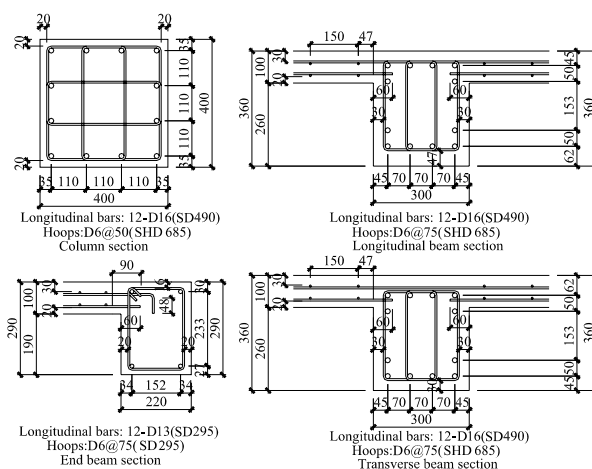


Figure 2. Geometry of the specimen

Slab reinforcements were D6 (SD295)@150 in both directions. The columns had 12-D16 (SD490) as main reinforcements (the gross ratio was 1.51%) and D6 (SHD685)@50 as hoops as shown in Fig. 3. The beams had 6-D16 (SD490, 2 lines) as top main reinforcements and 6-D16 (SD490, 2 lines) at the bottom (the gross ratio is 2.23%). The stirrups in the beams were D6 (SHD685)@50. The main

reinforcements of all the column and beam were anchored by welding with 40mm thick steel plates at the ends. Casting of concrete was divided into three times as in the parts of: 1) lower columns and joints, 2) beams and slabs, and 3) upper columns. The construction joints were placed about 75mm away from the column faces with wire mesh.



**Figure 3.** Column and beam sections

## 2.2. Materials

In order to simulate middle stories of high-rise buildings, high strength materials were utilized in this specimen. The results of material tests are shown in Table 1 and Table 2. The D16 bars used as the longitudinal reinforcements of beams and columns had a distinct yield plateau region, while the D6 bars used as the reinforcements of slabs and hoops did not have a yield plateau region.

**Table 1.** Results of concrete material tests

Concrete	Compressive strength	Strain at peak strength	Elastic Modulus	Tensional strength
	N/mm <sup>2</sup>	$\mu$	N/mm <sup>2</sup>	N/mm <sup>2</sup>
Lower columns and joints	75.98	2758	35739	5.02
Beams and slabs	65.73	2653	33072	4.85
Upper columns	67.40	2701	35083	4.61

**Table 2.** Results of reinforcement material tests

Steel bars	Yield strength	Yield strain	Elastic Modulus	Peak strength
	N/mm <sup>2</sup>	$\mu$	N/mm <sup>2</sup>	N/mm <sup>2</sup>
D16(SD490)	550.25	3277	204990	707.86
D6(SD295)	371.49	3981	185907	541.36
D6(SHD685)	712.82	5840	186305	910.09

## 2.3. Loading Method

The loading setup is illustrated in Fig. 4. In order to release the beam's axial forces caused by their elongation, the columns in south side were put on the pin supports, while the columns in north side were put on pin roller supports. The ends of half-spans in both sides were supported by pin load cells simulating the inflection points at mid-span. In addition, two 200mm by 200mm steel beams were appended on the end beams strengthening their stiffness. Vertical jacks pinned with columns could move freely by the roller supports on the top. Seismic loads were applied to the column tops by four jacks and to the pin roller supports at the bases by two jacks.

The details of the column pin support and pin roller support at the column bases were shown in Fig. 5. Steel footing of pin support was fixed on the foundation, while steel footing of pin roller support was just put on a smooth plastic plate so that transversal movement was allowed. Steel rods of  $\Phi 75$  welded on the steel footing were attached with the column faces to apply horizontal force or reactions. Two smooth steel curve face plates with a radius of 750mm were manufactured. One was connected to the column bottom, and another one was just put under it and could move freely with the rotation of column. Nevertheless, in the process of test, these supports did not work well as anticipated possibly due to the friction or precision of manufacture, details of which will be discussed later.

To simulate the vertical loads of high-rise buildings, the columns were subjected to constant axial force of 900kN each by four vertical actuators. Averaged compressive stress of the column section was 0.084 times the concrete strength. Static lateral cyclic forces were applied with six lateral oil jacks. The south jacks and north jacks were operated respectively. The story drifts were synchronized between south columns and north columns controlled manually through timely feedback data from displacement meters. Fig. 6 shows the story drift ratio history up to maximum value of 0.06rad.

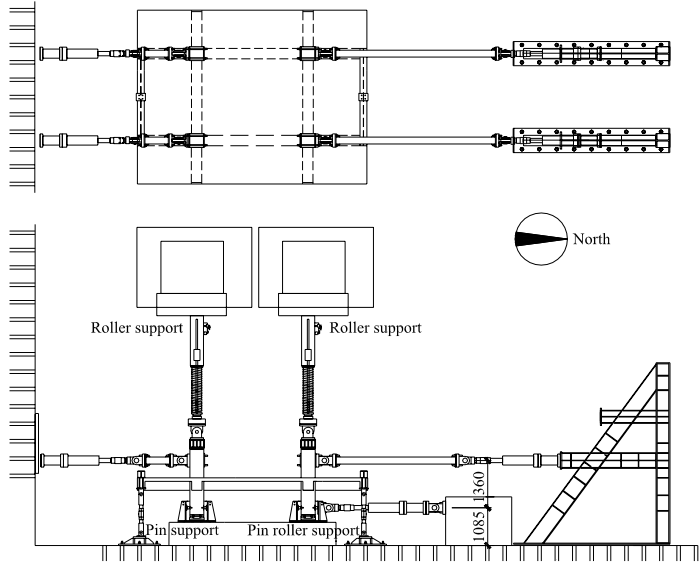


Figure 4. Loading set up

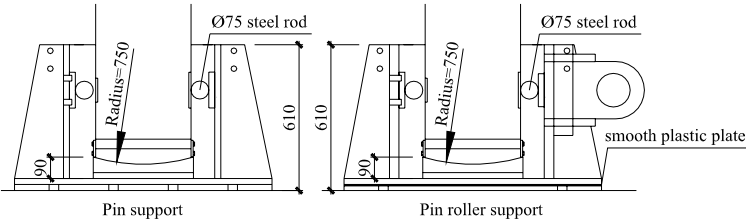


Figure 5. Pin support and pin roller support

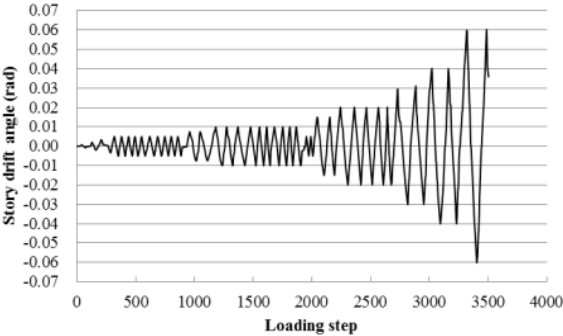


Figure 6. History of story drift ratio

### 3. TEST RESULTS AND DISCUSSION

#### 3.1. Observed response

The overall hysteretic relation of story shear force and story drift ratio is displayed in Fig. 7. The peak story shear force is 1963kN reached in 0.02 drift ratio. After the peak point, the specimen still exhibited ductile behavior without sharp reduction in strength.

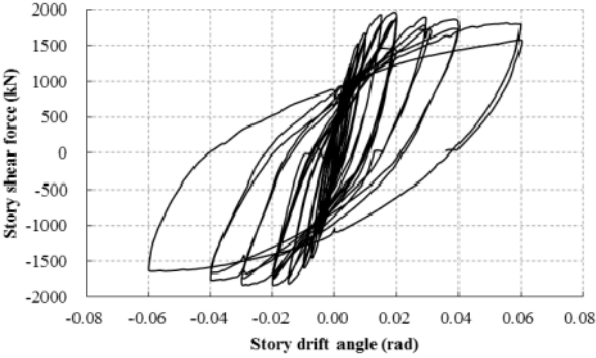


Figure 7. Load displacement relation

During the loading process of first loading cycle (1/1000), cracks initiated in a vertical type(bending type) from beam's bottom near joints when the story shear force are 227kN (positive load direction) and 247kN (negative load direction). All the initial cracks were about 75mm away from the column's face due to the construction joints. At the peak of 3/1000 cycles, inclined cracks (shear type) developing from beam's bottom were observed in the middle span. However, there were almost no obvious inclined cracks from the beam bottom on side half-spans in the whole loading process. This is because that the inflection point of middle span was moved to hogging moment side for slab participation, causing smaller shear span ratio that tend to generate shear cracks. The crack pattern of beam side in 1/200 cycle and 1/100 cycle were shown in Fig. 8.

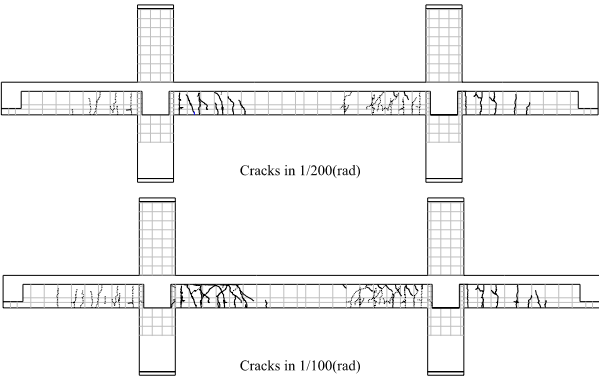


Figure 8. Cracks on beam

In 1/100 cycle, cracks were founded on the column side faces above joints, and they became more and wider with the increasing of story drift. However, no cracks were found on the column side faces below the joints in the whole process of the test. Moreover, it was observed that the inclination of the upper columns was larger than the lower columns, which was more obvious in larger story drift. Actually, bending moments had occurred at the base of all the columns. It also could be proved by the deformation of columns and strain of reinforcements as introduced in the next part. In the case that curve face steel plate did not move to the exact place, the reaction of column's base would not locate on the center axis of column. Thus, the eccentric of bottom reaction would generate a large moment because of the high axial force in column.

The side half-spans of the transverse beams were observed having cracks on beam side near joints from 1/1000 cycle. However, these cracks were also exactly at the place of construction joints. In addition the width and number of cracks on transverse beam almost remain unchanged until 1/50 cycle. It proves that stiff boundary conditions were provided for the slab. After 1/50 cycle, inclined cracks were started to form on transverse beams and the width became wider.

The cracks in the slab were firstly observed on the top face of slab in the peak of 2/1000 cycle. However, as the initial crack in slab, it penetrated the whole width of slab immediately. Cracks on the bottom face of slab were also observed in 3.3/1000 drift of positive load direction and 2/1000 drift in the negative load direction. The cracks of middle span were perpendicular to the longitudinal beams, while cracks on the side half-spans inclined due to the different boundary conditions. The crack pattern on the slab's top face in 1/200 cycle and 1/100 cycle were displayed in Fig. 9. Another phenomenon is that when slab cracks propagated to beams, the primary cracks in vertical type would be changed to an inclined type from slab bottom.

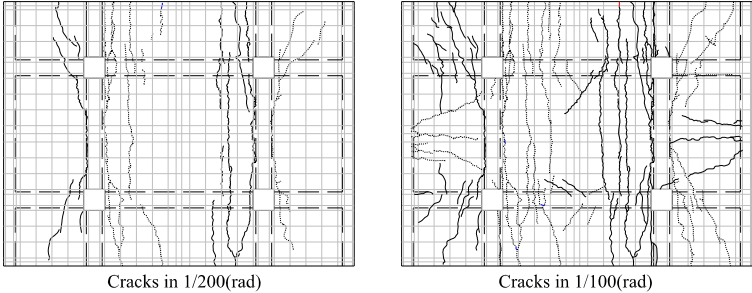
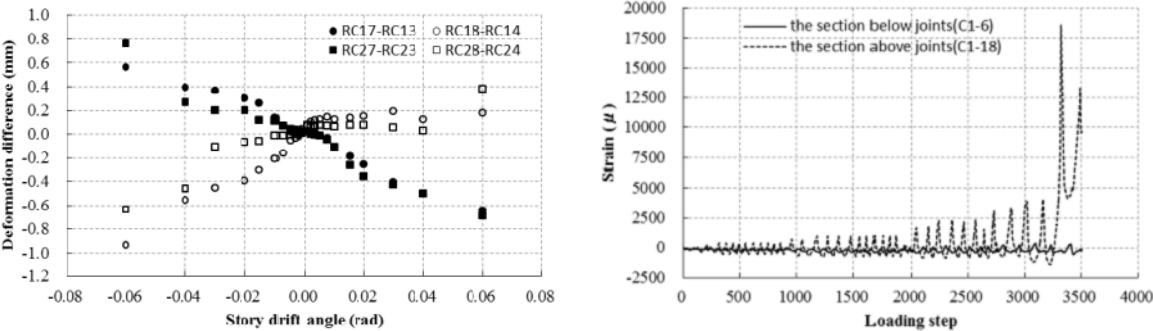


Figure 9. Cracks on the slab's top face

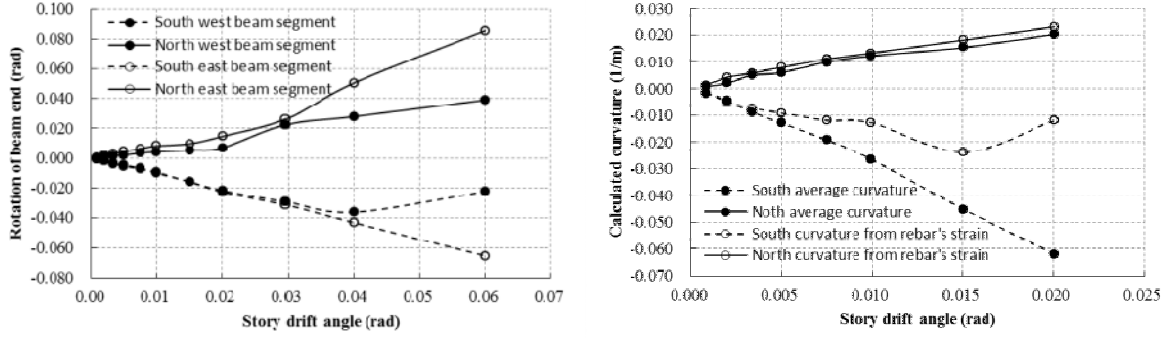
3.2. Deformation and strain

Due to the column base moments, inflection points were found in the lower columns. Opposite deformation tendency was indicated between the two segments of the lower columns in Fig. 10 (a). Strains in the main bars of the section below joints were also much less than the section above joints. Fig. 10 (b) shows typical strain history of the corner bar in the south west column above and below the joint. The beam end rotation of middle span in positive load direction was shown in Fig. 11 (a). The rotation of the hogging moment was slightly larger than sagging moment until 0.02 drift ratio. According to measured strains, the beam bottom bars yielded at 0.015 drift ratio, beam top bars yielded at 0.02 drift ratio. Fig. 11 (b) shows two types of the beam end curvatures: one was the average rotation of the 350mm length of beam end in positive load direction and another one was calculated from beam reinforcement strain at the beam end section in the positive load direction. South curvature calculated by reinforcement strain is less than averaged obviously, which means that actual strains in the beam bottom bars were much larger than measured from strain gauges.



(a) Deformation difference in lower column (b) Strain of the column main bar

Figure 10. Evidence of base moment in the test results



(a) Beam rotation in positive loading direction (b) Beam curvature in positive loading direction  
**Figure 11.** Comparison of beam rotation and curvature

### 3.3. Strength of specimen

To investigate the strength of the specimen, proper evaluation of the column base moments was essential. The strains measured in the lower column bars were no more than  $600\mu$  both in tension and compression until 0.02 drift ratio. Therefore, elastic curvature distribution could be assumed to the lower columns, which was proportional to the moment distribution. The force of the lower columns could be simplified as a cantilever subjected by a horizontal force  $F$ , a moment  $M$  and a axial force  $N$  as shown in Fig. 12. The rotation angles of the two segments measured by displacement meters could be used to solve the relationships between the horizontal forces and the base moments.

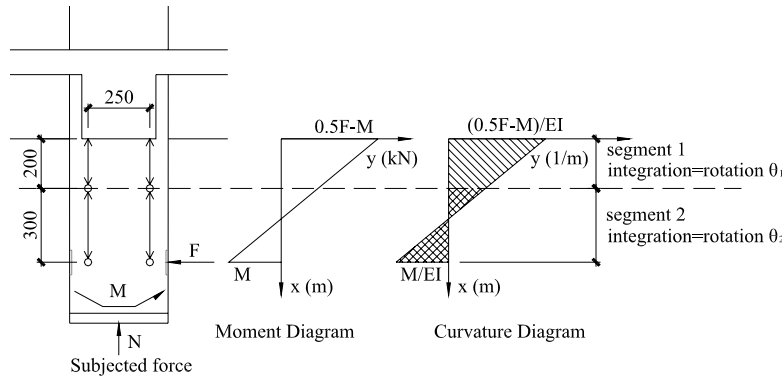


**Figure 12.** Estimate model of base moment

Eqn. 3.1 presents the moment along the axis  $x$  in Fig. 12 and Eqn. 3.2 presents the curvature along the axis  $x$ . By integrating the curvature for the segment 1 and segment 2, the rotations of two segments  $\theta_1$  and  $\theta_2$  could be solved as Eqn. 3.3 and 3.4. Meanwhile,  $\theta_1$  and  $\theta_2$  also could be derived from the deformation of column by displacement meters. Through computing the ratio of  $\theta_1$  between  $\theta_2$ , the relations of the base moment and the base horizontal force could be derived as Eqn. 3.5.

$$M(x) = F(0.5-x) - M \quad (3.1)$$

$$\Phi(x) = (0.5F - M - Fx) / EI \quad (3.2)$$

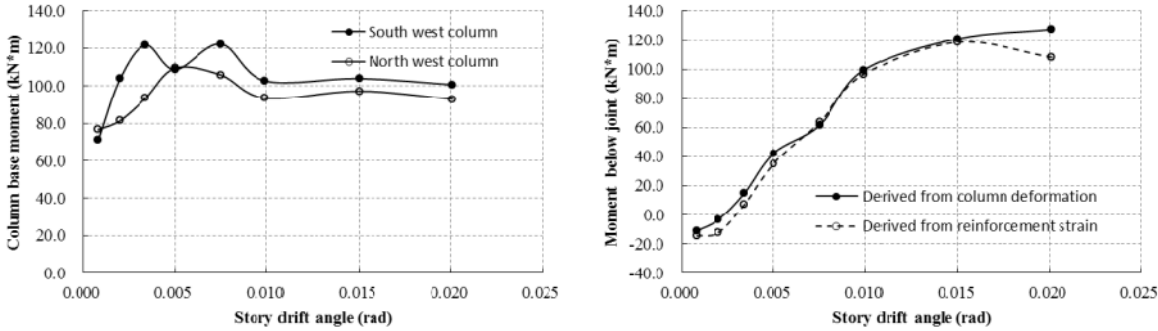
$$\theta_1 = \int_0^{0.2} \Phi(x) dx = (0.08F - 0.2M) / EI \quad (3.3)$$

$$\theta_2 = \int_{0.2}^{0.5} \Phi(x) dx = (0.045F - 0.3M) / EI \quad (3.4)$$

$$(0.08F - 0.2M) / (0.045F - 0.3M) = \theta_1 / \theta_2 \quad (3.5)$$

The base moments of the south-west and north-west columns were calculated from Eqn. 3.5 at the first peaks of the loading cycles as shown in Fig. 13 (a). The moments at the lower section under the joint

in the south-west column were derived from these calculated base moments as shown in Figure 13 (b). To confirm the reliability of these calculated results, another method, computing the moment by the strains of column main bars were also implemented. Linear strain distribution was assumed at the section. The maximum compressive strain of bars was used to estimate the strain of concrete. Then, other strain distributions were estimated from the strain at this point and the total axial force. The section moments derived by measured strains were obtained as also shown in Fig. 13 (b). The figure indicates that both estimation methods gave close results. After the determination of the column base moments, the whole moment distribution could be obtained including the beam ends.



(a) Column base moment (b) Moment of the section below joint

Figure 13. Estimate of base moment

4. ANALYSES BY FINITE ELEMENT MODEL

4.1. Analytical models

The relations between the inter-story drift and the effective width of slab were demonstrated with finite element model analysis of the test specimen. The element division and boundary conditions of the analytical model are shown in Fig. 14. The fibre elements of the floor slab were idealized with Timoshenko beam elements in the longitudinal direction, which were jointed with elastic springs in the transverse direction. The number of elements was 15 in the internal longitudinal girder, 8 in the outer longitudinal girder, 14 in the internal transverse girder, and 8 in the outer transverse girder. These girders are idealized with beam elements as used in the floor slab. The model ignores attached columns, and external bending moment is applied to the beam-column joints being solid elements.

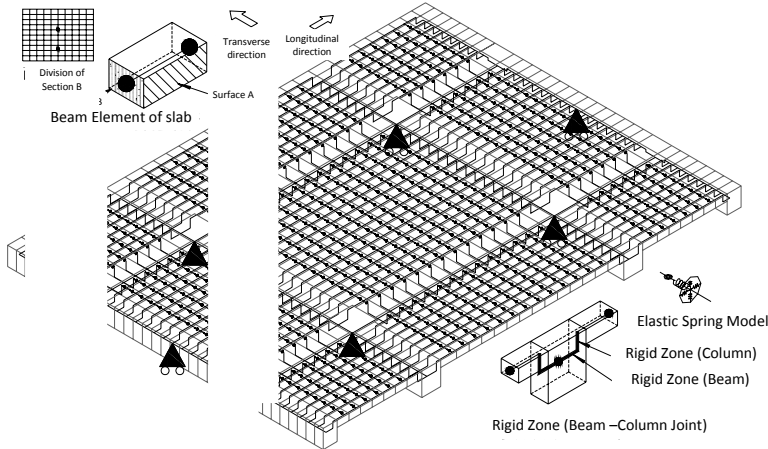


Figure 14. Finite Element Model

The shear locking mechanism was eliminated by reduced integration method. Once concrete crack

occurs due to tensile strain, the tensile strength of concrete fibre was released. The out of plain deformation of the concrete slab by shear and torsional moment, and in-plane deformation of concrete slab by torsional moment represents by the elastic response of the lower concrete slab surface. In order to equalize in-plane deformations with shell elements model, the stiffness of the elastic spring in the transverse direction was decreased from the axial stiffness of concrete. The reduced factor  $k$  was taken as 0.2 based on the comparison of observed elastic deformation distribution with analytical models in this study. The tensile strength of concrete was ignored after the concrete crack occurred at the tensile strain of 0.00012.

**4.2. Analyses result**

The elongation of the longitudinal beam in the inner span was shown in Fig. 15. The strain and stress distributions in the transverse slab section are shown in Fig. 16. Fig. 17 (a) shows the relations between the inter-story drift and the sagging moment at the beam critical section. The relation between inter-story drift ratio and the ratio of effective slab width to the span length (the effective width ratio) was derived from the axial stress distributions of the beam elements. The ratios of the longitudinal beams in the inner span are shown in Fig. 17(b).

The effective width ratio is 0.64 in 0.005(rad), and 0.97 in 0.010(rad) in this specimen. Therefore, the effective slab width is much larger than adopted in the conventional Japanese structural design in the calculation of the ultimate lateral load carrying capacity, where 1m in full-scale (400mm in the specimen) at one side is being taken, which corresponded to  $0.8/2.5=0.32$  in term of the effective slab ratio defined as above. The analytical and experimental results might have been derived because (1) the tensile stiffness reduced in the longitudinal direction due to concrete cracking, (2) the strain was averaged in beam and slab section by the elongation in the longitudinal direction, and (3) the axial stress distribution was smoothed by preceding yield of slab reinforcements.

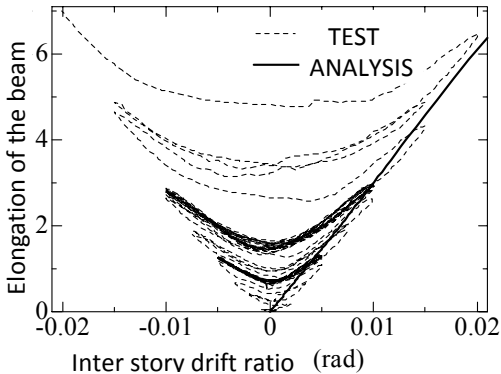


**Figure 15.** Relation between inter-story drift ratio and beam elongation

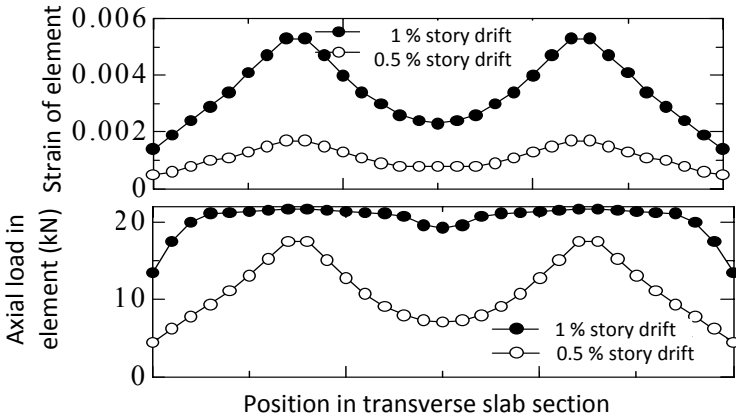
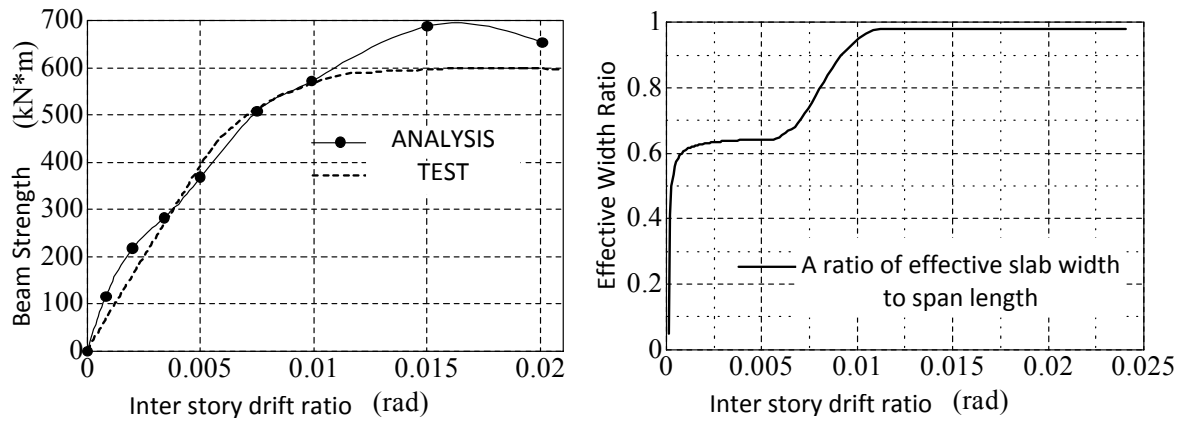


**Figure 16.** Stress/strain distribution in transverse slab section



(a) Beam strength against sagging moment

(b) Effective width ratio of floor slab

**Figure 17.** Beam strength and effective width ratio in FEM analysis

## 5. CONCLUSION

Test and analysis were conducted on the effective slab width to the ultimate strengths of the beams in the three-dimensional reinforced concrete frame, from which the followings could be drawn:

- (1) The crack patterns observed on the slab were obviously influenced by the boundary conditions of the specimen and loading. For the interior part of the buildings, the sagging moments and the beam elongations produced straight cracks on the slab in parallel to the transverse beam on the slab, while the cracks in the outer parts inclined perpendicular to the radiating forces from the reaction points at the centre of the boundary beams.
- (2) The transverse strains measured in the slab reinforcement along the critical section did not decrease with the increase of the distance from the central axis of the frame. Consequently, the slab reinforcing bars were nearly fully effective to the beam ultimate flexural moments at the story drift of 0.010(rad), which was also consistent with the calculated and measured ultimate flexural resistances of the frame taking estimated moment reactions at the column bases into account.
- (3) The relations between the beam strengths and the inter-story drift were evaluated also by a finite element analysis model, from which the ratio of the effective slab width to the whole width was evaluated as 0.64 at the story drift of 0.005(rad), and up to 0.97 at 0.010(rad), which was much higher at lower drift levels than assumed in the current design practice and observed in the past tests.

## ACKNOWLEDGEMENT

This study was supported by the subsidies for the project of servicing the architectural standard from the Ministry of Land, Infrastructure, Transport and Tourism. And also this study was carried out under the cooperation and advice from the committee of study on seismic safety for RC structures under long-period ground motions. The support and cooperative works for the research are gratefully acknowledged.

## REFERENCES

- Suzuki, N., Otani, S. and Kobayashi, Y. (1984). "Three-Dimensional Beam-Column Subassemblages under Bidirectional Earthquake Loadings", *Proceedings, 8th WCEE*, **V. 6**: 453-460
- Sakata, H. and Wada, A. (1989). "Experiments on reinforced concrete one-twentieth scale model frames: A study on elastic and plastic behaviors of reinforced concrete frames in consideration of axial elongation in bending yield beams," *Journal of Structural and Construction Engineering*, **AIJ (403)**: 45-55
- Kabeyasawa, T., Fukuyama, H., Katsumata, H., Sugimoto, K., Kabeyasawa, T., Xuan, D. (2012). "Static loading test of a three-dimensional frame simulating high-rised reinforced concrete building structures (No.1: Outline of the test), *Proceedings, AIJ Annual Convention*, **C-2**:741-742.